

## Deposition rate enhancement in HiPIMS without compromising the ionized fraction of the deposition flux

This article has been downloaded from IOPscience. Please scroll down to see the full text article.

2013 J. Phys. D: Appl. Phys. 46 205205

(<http://iopscience.iop.org/0022-3727/46/20/205205>)

View [the table of contents for this issue](#), or go to the [journal homepage](#) for more

Download details:

IP Address: 158.64.77.38

The article was downloaded on 07/05/2013 at 14:07

Please note that [terms and conditions apply](#).

# Deposition rate enhancement in HiPIMS without compromising the ionized fraction of the deposition flux

J Čapek<sup>1,2</sup>, M Hála<sup>1</sup>, O Zabeida<sup>1</sup>, J E Klemberg-Sapieha<sup>1</sup> and L Martinu<sup>1</sup>

<sup>1</sup> Department of Engineering Physics, École Polytechnique de Montréal, PO Box 6079, Station Downtown, Montreal, Quebec H3C 3A7, Canada

<sup>2</sup> Department of Physics, University of West Bohemia, Univerzitni 22, 30614 Plzen, Czech Republic

E-mail: [jcapek@kfy.zcu.cz](mailto:jcapek@kfy.zcu.cz)

Received 4 January 2013, in final form 5 March 2013

Published 2 May 2013

Online at [stacks.iop.org/JPhysD/46/205205](http://stacks.iop.org/JPhysD/46/205205)

## Abstract

We systematically investigate and quantify different physical phenomena influencing the deposition rate,  $a_D$ , of Nb coatings prepared by high power impulse magnetron sputtering (HiPIMS), and propose a straightforward approach for deposition rate enhancement through the control of the magnetron's magnetic field. The magnetic field strength at the target surface,  $B$ , of a 50 mm diameter magnetron was controlled by the application of paramagnetic spacers with different thicknesses in between the magnetron surface and the target. We found that lowering  $B$  achieved by the application of a 2.8 mm thick spacer led to an increase in  $a_D$  by a factor of  $\sim 4.5$  (from 10.6 to 45.2 nm min<sup>-1</sup>) when the discharge was operated at a fixed average pulse target power density (2.5 kW cm<sup>-2</sup>). However, the ionized fraction of the deposition flux onto the substrate was found to be comparable, despite a large difference in  $B$ -dependent discharge characteristics (magnetron voltage and discharge current). We show that the decrease in  $a_D$  commonly observed in HiPIMS (ranging from 33% to 84% in comparison with dc magnetron sputtering in the presented experiments) is governed by different physical processes, depending on the value of  $B$ : for high  $B$ , the back-attraction of the target ions towards the target is the dominant effect, while for low  $B$  the ion back-attraction, the sub-linear dependence of the sputtering yield on the ion energy, and the variation in material transport effects are all important. Finally, we offer a theoretical background for the observed results, demonstrating that the here-presented conclusions may be applicable to HiPIMS discharges using different metal targets and different inert gases.

(Some figures may appear in colour only in the online journal)

## 1. Introduction

High power impulse magnetron sputtering (HiPIMS) is a pulsed direct current sputtering technique utilizing high instantaneous peak power densities of typically several kilowatts per square centimetre applied at a low repetition frequency, in order to protect system components (e.g. sputtered target and/or magnets inside the magnetron) against overheating. The high instantaneous power results in a high density discharge and, consequently, in a high ionized fraction of the deposition flux onto the substrate, which opens new attractive possibilities for enhancing and tailoring coating properties [1–3].

It has been found that the deposition rate,  $a_D$ , in non-reactive HiPIMS is typically only 30–85% of the value encountered in (non-pulsed) direct current magnetron sputtering (DCMS) operated at the same average discharge power [4, 5]. The origins of the drop in  $a_D$  have been intensively investigated over the last several years. While no unique explanation has been developed until now, the following phenomena influencing  $a_D$  in a non-reactive HiPIMS (excluding HiPIMS above hot targets [6]) have been considered: (i) *yield effect*—a decrease in  $a_D$  due to a sub-linear energy dependence of the sputtering yield [7]; (ii) *return effect*—a decrease in  $a_D$  caused by enhanced ionization of sputtered atoms and by their back-attraction to the target [8];

(iii) *species effect*—a change in  $a_D$  corresponding to working gas ions replacement by the back-attracted target material ions exhibiting a different sputtering yield [9]; (iv) *transport effects*—a change in  $a_D$  caused by a modified transport of the sputtered target material particles (ions and/or neutral atoms) towards the substrate [10]; (v) *coating effects*—a lower  $a_D$  due to an increased coating density, a reduced sticking coefficient and a possible etching of the growing coating [5, 9].

Despite all the efforts that have been devoted to the understanding of individual phenomena, a general unified approach for the enhancement and optimization of the sputtered material flux towards the substrate (without losing the benefits of HiPIMS) is still missing. In this context, our preliminary work and few recent papers appear to suggest that controlling the strength of the magnetron's magnetic field at the target surface,  $B$ , is a promising optimization pathway. For example, Ehiasarian and Vetushka [11] demonstrated that a reduction in  $B$  from 50 down to 25 mT enhances the deposition rate of Cr coatings by more than 30%. In addition, Mishra *et al* [12] reported that the deposition rate of Ti films could be increased up to six times by weakening  $B$  by 33%. However, the concept of the effect of the magnetic field on the deposition rate has yet to be fully explored and explained.

In this work, we systematically investigate the effect of  $B$  on the sputtered material flux travelling towards the substrate as well as backwards to the target, in the specific case of a non-reactive HiPIMS discharge operated above a Nb target. This allows us to propose a straightforward concept for a HiPIMS deposition rate enhancement by an adjustment of the magnetron's magnetic field that can then be applied to achieve the optimal HiPIMS discharge operation conditions.

The choice of Nb as a model target material in this study was made due to interesting superconducting properties of Nb-based alloys [13], and due to the formation of an attractive high refractive index oxide when sputtered in reactive Ar/O<sub>2</sub> gas mixture [14]. However, it will be shown that the here-presented findings and conclusions may be valid for any material in general.

In the first part, we study the discharge characteristics and the deposition rate for various  $B$ , characterized by different combinations of magnetron voltage,  $U_d$ , and target current density,  $J_d$ . Subsequently, we quantify the above-listed phenomena influencing the sputtered material flux and thus  $a_D$ , in the case of two distinct magnetic field strengths (high  $B$  and low  $B$ ). We then elaborate in detail on the ionized fraction of the sputtered material at the substrate level. Finally, we provide a theoretical explanation of the experimental observations by adopting the phenomenological model proposed by Vlček and Burcalová [15].

## 2. Experimental setup

All experiments were carried out in the vacuum deposition system illustrated in figure 1(a) using a grounded stainless-steel chamber, in a pure Ar atmosphere at pressure,  $p = 1$  Pa. An unbalanced magnetron (the magnetic field structure is shown in figure 1(b)) equipped with a 5 cm diameter Nb

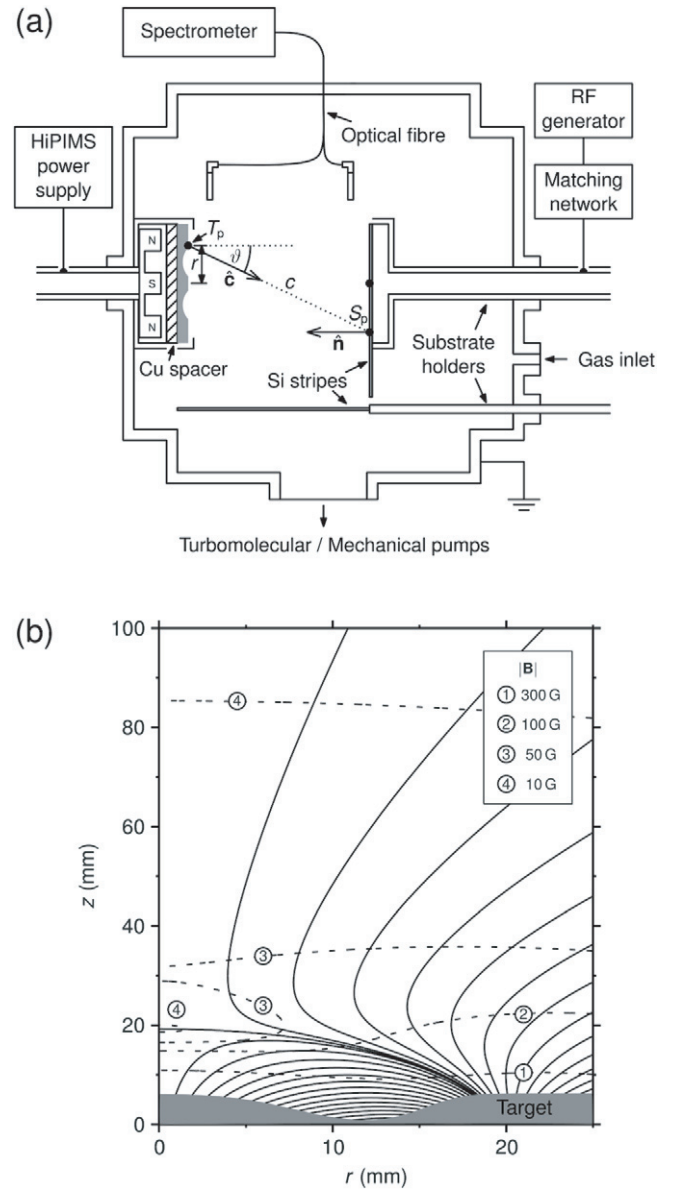


**Figure 1.** Schematic diagram of the experimental setup (a) and magnetic field lines (solid lines) and contours of the magnetic field,  $|B|$ , (dashed lines) of the 50 mm diameter unbalanced magnetron used in this work (b).

target was powered by a HÜTTINGER Electronics HMP2/1 power supply (2 kW maximum average power) working in the frequency range from 2 to 500 Hz, at a voltage pulse duration between 1 and 200  $\mu$ s and with a maximum voltage and peak current of 2 kV and 1000 A, respectively. The pulse repetition frequency  $f_r = 50$  Hz and the voltage pulse duration  $t_1 = 200 \mu$ s (duty cycle  $t_1/T = 1\%$ , pulse period  $T = 1/f_r$ ) were used in order to achieve very high power densities during the individual pulses at low total (average) powers. The average target power density in a period,  $\bar{P}_d$ , and the average pulse target power density  $P_{da}$  (due to the fixed repetition frequency and fixed pulse duration) were kept constant in all experiments at  $25 \text{ W cm}^{-2}$  and  $2.5 \text{ kW cm}^{-2}$ , respectively. For comparison purposes, some experiments were carried out using a (non-pulsed) dc power supply, Advanced energy MDX (maximum voltage of 1.0 kV

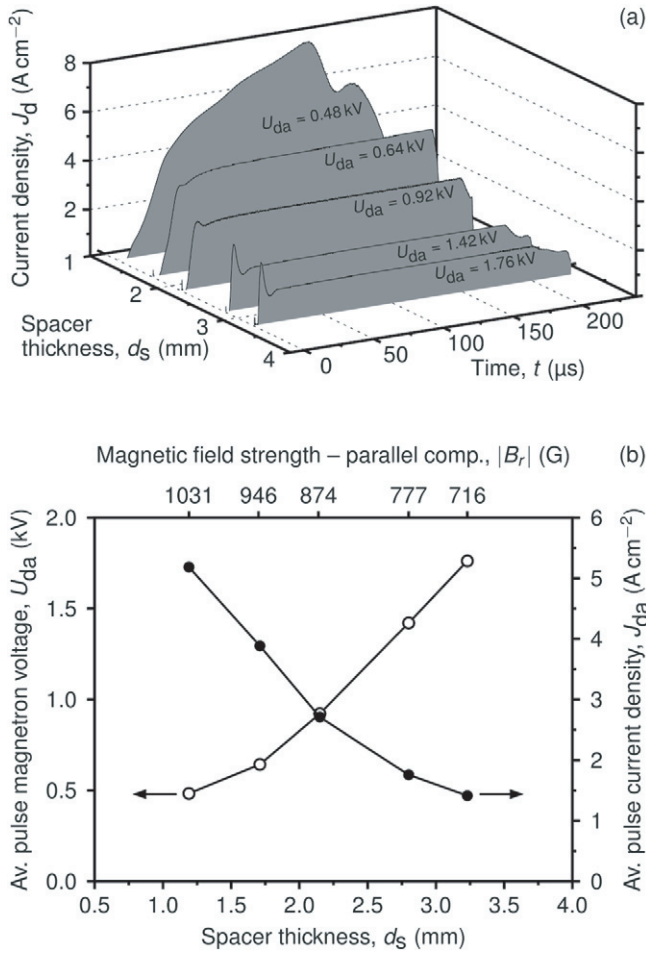


**Figure 2.** Waveforms of the target current density  $J_d$  obtained at a constant average pulse target power density  $P_{da} = 2.5 \text{ kW cm}^{-2}$ , and plotted as a function of copper spacer thickness  $d_s$  in between the Nb target and the magnetron head (a). The corresponding average pulse values of the target current density  $J_{da}$  and of the magnetron voltage  $U_{da}$ , are plotted as a function of spacer thickness  $d_s$  (b).

and maximum discharge current of 1 A) at the same average target power density in a period  $\overline{P_d} = 25 \text{ W cm}^{-2}$ .

In this work, the magnetron’s magnetic field strength at the target surface was modified by applying copper spacers in between the target and the magnetron head. The Nb target was highly eroded (80% of target erosion [16]) in order to reach very high instantaneous target current densities (up to  $8 \text{ A cm}^{-2}$ ) in the case of a thin spacer. The thickness,  $d_s$ , of the used spacers was in the range 1.2 to 3.2 mm. This variation in the total target thickness allowed to reach significantly different values of the average pulse magnetron voltage  $U_{da}$  (ranging from 0.48 to 1.76 kV) and of the corresponding average pulse target current density  $J_{da}$  (ranging from 1.4 to  $5.2 \text{ A cm}^{-2}$ ), at the constant average pulse target power density  $P_{da} = 2.5 \text{ kW cm}^{-2}$  (see figure 2).

Waveforms of the discharge voltage  $U_d(t)$  and of the target current  $I_d(t)$  were measured by a Tektronix P6015A voltage probe and a Pearson 301X current monitor, respectively, and recorded by a Tektronix TDS2014B digital oscilloscope. Subsequently, our own software was used to evaluate

the average pulse magnetron voltage as

$$U_{da} = \frac{1}{t_1} \int_0^{t_1} U_d(t) dt; \quad (1)$$

the average pulse current density as

$$J_{da} = \frac{1}{t_1 A_t} \int_0^{t_1} I_d(t) dt, \quad (2)$$

where  $A_t$  stands for the total target area ( $\sim 20 \text{ cm}^2$  in our case). The average pulse target power density is then expressed as

$$P_{da} = \frac{1}{t_1 A_t} \int_0^{t_1} U_d(t) I_d(t) dt. \quad (3)$$

Note that the average target current density in a period,  $\overline{J_d}$ , and the average target power density in a period,  $\overline{P_d}$ , were calculated using the same formulae as for the corresponding pulse values, but integrated over the whole pulse period.

Nb coatings were prepared on Si(1 0 0) substrates kept at ambient temperature, positioned at a distance  $d = 10 \text{ cm}$  from the target. The substrate holder (surface area  $\sim 50 \text{ cm}^2$ ) was biased to  $-20 \text{ V}$  by an Advanced Energy RF 600 power supply in order to eliminate the discharge ignition delay without affecting the resulting steady-state current value. Depositions on silicon stripes fixed parallel and perpendicular to the target surface (see figure 1) were also carried out in order to determine the relative angular distribution of the sputtered material. The thickness of the fabricated films was measured by a Veeco Dektak 3030ST Profilometer equipped with a conical diamond stylus.

A Sartorius Le225D balance (capacity 220 g and readability 0.01 mg) was used for the measurement of the target mass before and after deposition.

Finally, optical emission spectra from the discharge were collected by an optical fibre probe mounted within the reactor overlooking the discharge at the distances of  $d = 1 \text{ cm}$  and  $d = 9 \text{ cm}$  from the target. Its line of sight was parallel with the target surface. The time-averaged optical spectra were recorded by Ocean Optics USB2000 spectrometer.

### 3. Results and discussion

#### 3.1. Discharge characteristics and Nb deposition rate

In our recent work [16], we have demonstrated that the target current density of a steady-state high density discharge in front of a Nb target can be effectively reduced by decreasing  $B$ . This was accomplished by applying paramagnetic spacers of different thicknesses in between the magnetron’s surface and the eroded target. This technique is also used in this work, in order to reach significantly different combinations of  $U_d$  and  $J_d$  at a constant average pulse target power density  $P_{da} = 2.5 \text{ kW cm}^{-2}$ .

Steady-state high density discharges were obtained in practically all investigated conditions except the experiment with 1.2 mm thick spacer (see figure 2(a)). In this particular case,  $J_d$  is too elevated for the power supply’s capacitors [16, 17], and thus, the pure steady-state conditions was not

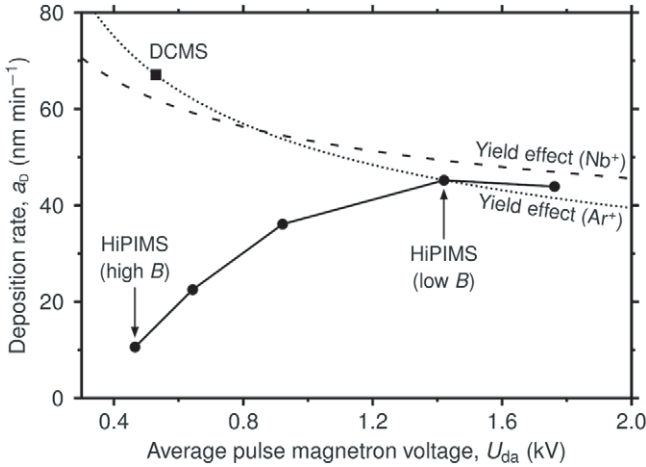


**Figure 3.** Deposition rate of Nb coatings  $a_D$  as a function of average pulse magnetron voltage  $U_{da}$  obtained at a constant average pulse target power density  $P_{da} = 2.5 \text{ kW cm}^{-2}$  (circles). Deposition rate corresponding to a dc discharge operated at the same average target power density in a period,  $\overline{P_d} = 25 \text{ W cm}^{-2}$ , is plotted for comparison (square). Moreover, a theoretical drop in the deposition rate caused by the sub-linear dependency of the sputtering yield on magnetron voltage is indicated for a flux of Ar ions (dotted line) and of Nb ions (dashed line).

reached. For this reason, we discuss the results as a function of the average pulse values (indicated by the subscript ‘a’ in the notation, see equations (1)–(3)). It should be also noted that introducing thicker spacers ( $d_s > 3.2 \text{ mm}$ ) inhibits reaching the desirable  $P_{da}$  value for magnetron voltages up to 2 kV (power supply’s limit).

As depicted in figure 2(b), the advanced erosion state of the target (80%), in combination with the 1.2 mm thick spacer, results in very high  $J_{da} = 5.2 \text{ A cm}^{-2}$  at a relatively low  $U_{da} = 0.48 \text{ kV}$ . In contrast, a gradual increase in the spacer thickness up to 3.2 mm leads to a distinct drop in  $J_{da}$  (down to  $1.4 \text{ A cm}^{-2}$ ) at high  $U_{da} = 1.76 \text{ kV}$ . Let us emphasize that both discharge characteristics,  $J_{da}$  and  $U_{da}$ , are thus varied by a maximum factor of  $\sim 3.7$ . This significant variation of the discharge characteristics greatly affects the Nb deposition rates.

Figure 3 shows  $a_D$  of Nb coatings prepared by HiPIMS at various  $B$  values (circles), and by DCMS at low  $B$  (square), measured in the centre of the substrate holder. One can see that  $a_D$  of the HiPIMS-deposited Nb films increases from  $10.6 \text{ nm min}^{-1}$  at  $U_{da} = 0.48 \text{ kV}$  (corresponding to high  $B$ ) up to  $45.2 \text{ nm min}^{-1}$  at  $U_{da} = 1.42 \text{ kV}$  (corresponding to low  $B$ ). In fact, the deposition rate is enhanced by a factor of  $\sim 4.5$ , and reaches 67% of the DCMS rate ( $a_D = 67.1 \text{ nm min}^{-1}$ ) at the optimum (low)  $B$ . These experimental observations clearly demonstrate that it is possible to enhance (maximize) Nb’s deposition rate by a simple control of  $B$ . A general discussion and a corresponding theoretical explanation will be offered in section 3.4.

### 3.2. Physical phenomena affecting the deposition rate

Understanding the changes in  $a_D$  shown in figure 3 requires a detailed analysis in which all the phenomena summarized in

section 1 are considered. In the following we systematically investigate the physical factors that affect the deposition rate, in the order in which the sputtered matter travels: from the target surface, into the space in between the target and the substrate, and finally at the substrate level.

**3.2.1. Sputtering conditions at the target: yield and species effects.** Let us describe the sputtering process of the target using the average target sputtering rate density in a period,  $\overline{R_Y}$ , defined as

$$\overline{R_Y} = \frac{\overline{J_d}}{1 + \gamma_{se}} Y(E_i), \quad (4)$$

where  $\gamma_{se}$  is the secondary electron emission coefficient and  $Y$  stands for the sputtering yield of the target material for an impacting singly charged ion with a kinetic energy,  $E_i \approx e U_{da}$ . Note that the effect of multiply charged ions on the sputtering process is considered as low, and thus, can be neglected. One should consider that in HiPIMS the bombarding ion flux consists of both the process gas ion flux,  $G_t^+$ , and of the target material ion flux,  $M_t^+$ . This gives origin to the *species effect* ((iii) in section 1), if the sputtering yields corresponding to both types of ions are different. We can take this effect into account in equation (4), by substituting for  $Y$  an effective sputtering yield,  $Y_m$ , defined as

$$Y_m = Y_{mg}(1 - m_t) + Y_{mm}m_t. \quad (5)$$

Here,  $Y_{mg}$  and  $Y_{mm}$ , stand for the sputtering yield of process gas and target material ions, respectively. The parameter,  $m_t$ , defined as

$$m_t = \frac{M_t^+}{G_t^+ + M_t^+} \quad (6)$$

is the fraction of target material ions in the total ion flux onto the target. Note that  $Y_{mg}$  and  $Y_{mm}$  values for a given ion energy can readily be calculated using, for example, the SDTrimSP code [18].

Let us introduce the ratio  $f^{\text{Yield}} = \overline{R_Y}(\text{HiPIMS}) / \overline{R_Y}(\text{DCMS})$  that describes the level of the *yield effect* (considering constant  $\overline{P_d}$ ). Then we can write (assuming that  $m_t = 0$  in DCMS and that  $\gamma_{se}$  is constant for the investigated discharges) that

$$f^{\text{Yield}} = \frac{U_d^{\text{DCMS}}}{U_{da}^{\text{HiPIMS}}} \frac{Y_m(U_{da}^{\text{HiPIMS}}, m_t)}{Y_{mg}(U_d^{\text{DCMS}})}. \quad (7)$$

Consequently, the theoretical change in the deposition rate of HiPIMS discharges due to the *yield effect* can be expressed as

$$a_D(\text{HiPIMS}) = a_D(\text{DCMS}) f^{\text{Yield}}. \quad (8)$$

In order to determine the value of  $f^{\text{Yield}}$ , we first need to find the exact value of  $m_t$ . This we will do in the subsequent section. However, what we already know is that the amplitude of the expected drop in  $a_D(U_{da})$  due to the *yield effect* has to fall somewhere in between the two extreme cases: sputtering by  $\text{Ar}^+$  flux ( $m_t = 0$ ) and by  $\text{Nb}^+$  flux ( $m_t = 1$ ) (depicted by the respective curves in figure 3).

Figure 3 suggests that the *yield effect* might be the crucial phenomenon reducing the deposition rate at very high pulse

voltage values of  $U_{da} \geq 1.42$  kV (i.e. in the case of low  $B$ , when  $a_D$  reached about 33% of the DCMS rate). However, other effects lead to a significant decrease in  $a_D$  in the present experiments at lower pulse voltage values,  $U_{da} < 1.42$  kV (i.e. in the case of high  $B$ ). In order to better identify and distinguish all the important phenomena, further investigations were conducted. For the sake of simplicity, we will restrain the following discussion to three specific discharge conditions, highlighted in figure 3: (i) DCMS at low  $B$ , (ii) HiPIMS at high  $B$  and (iii) HiPIMS at low  $B$ .

In this work, we do not investigate or discuss the impact of  $B$  on  $a_D$  of DCMS-deposited films, since the latter is insignificant in comparison with the here-presented HiPIMS case. Under the discharge conditions used in this work the ionization of sputtered material in DCMS is low ( $\sim 1\%$  [19]), and thus, can be considered as negligible in the following discussion. For that reason, no *return* or *transport effects* need to be taken into account since magnetic or electric fields do not affect neutrals. The only possible change in  $a_D$  (DCMS) related to  $B$  can be attributed to the above-discussed *yield effect*. In fact, enhancing  $B$  will imply a decrease in  $U_d$  and a consequent increase in  $a_D$ , such as depicted by the dotted line for the  $Ar^+$  sputtering flux in figure 3. Moreover, let us recall that the discharge current in DCMS follows a power law  $I_d = a U_d^b$  with a significantly higher value of coefficient  $b$ , when compared with HiPIMS [1]. Therefore, a much lower decrease in  $U_d$  is anticipated in order to compensate a higher magnetic field (and hence higher current) if  $\overline{P_d}$  is to be kept constant.

**3.2.2. Return of the sputtered material.** Measurement of the target mass loss rate,  $M_r$ , offers valuable supplemental information about the sputtering process (since neither *transport* nor *coating effects* influence the measurement). As presented in figure 4,  $M_r$  significantly differs for the three investigated discharge conditions. The maximum target mass loss rate is reached for the DCMS discharge,  $M_r(\text{DCMS}) = 22.3 \text{ mg min}^{-1}$ , while both HiPIMS discharges exhibit much lower values  $M_r[\text{HiPIMS}(\text{high}B)] = 3.7 \text{ mg min}^{-1}$  (83% lower than  $M_r(\text{DCMS})$ ) and  $M_r[\text{HiPIMS}(\text{low}B)] = 8.5 \text{ mg min}^{-1}$  (62% lower than  $M_r(\text{DCMS})$ ).

Since very few sputtered metal atoms get ionized in the DCMS discharge, it is reasonable to assume that the *return effect* is negligible in this case. Then, the total target mass loss rate in HiPIMS can be expressed as

$$M_r(\text{HiPIMS}) = M_r(\text{DCMS}) f^{\text{Yield}} (1 - f^{\text{Return}}), \quad (9)$$

where  $f^{\text{Return}} = \beta\sigma$  is a probability that the sputtered material is ionized (probability  $\beta$ ) and attracted back (probability  $\sigma$ ).

Since the value of  $f^{\text{Yield}}$  can be calculated using equation (7), one can then easily determine  $f^{\text{Return}}$  as

$$f^{\text{Return}} = \frac{M_r(\text{DCMS}) f^{\text{Yield}} - M_r(\text{HiPIMS})}{M_r(\text{DCMS}) f^{\text{Yield}}}. \quad (10)$$

Before proceeding further, we first need to determine parameter  $m_t$ , in order to be able to determine the exact value

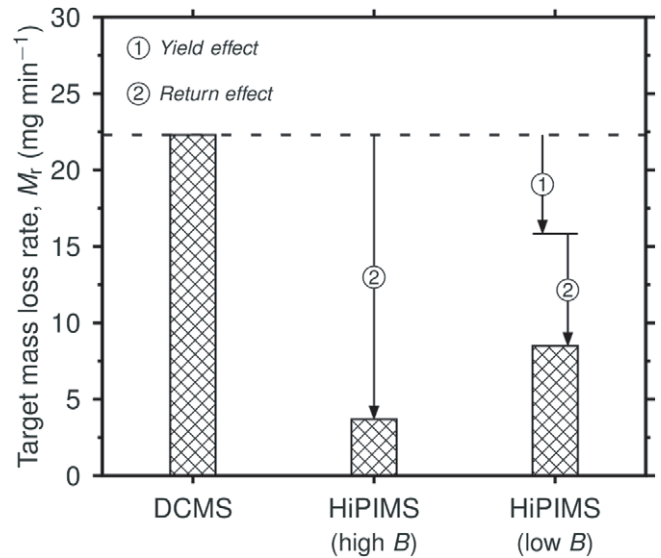


**Figure 4.** Mass loss rate of the niobium target for the DCMS discharge and for the two selected HiPIMS discharges (i.e. low and high magnetic field strength at the target surface), all operated at a constant average target power density in a period  $\overline{P_d} = 25 \text{ W cm}^{-2}$ . The *yield* and *return effects*' contributions are indicated for both HiPIMS discharges.

of  $f^{\text{Yield}}$ . Viček and Burcalová reported [15] in their model that  $m_t$  can be calculated as

$$m_t = \beta\sigma Y_m \equiv f^{\text{Return}} Y_m. \quad (11)$$

Combining equations (10) and (11), we find

$$m_t = \left[ \frac{M_r(\text{HiPIMS})}{M_r(\text{DCMS})} \frac{U_{da}^{\text{HiPIMS}}}{U_d^{\text{DCMS}}} Y_{\text{mg}}(U_d^{\text{DCMS}}) - Y_{\text{mg}}(U_{da}^{\text{HiPIMS}}) \right] \frac{1}{Y_{\text{mm}}(U_{da}^{\text{HiPIMS}}) - Y_{\text{mg}}(U_{da}^{\text{HiPIMS}}) - 1}. \quad (12)$$

Consequently we obtain  $m_t = 0.47$ ,  $f^{\text{Yield}} = 0.99$ ,  $f^{\text{Return}} = 0.83$  for the HiPIMS (high  $B$ ) discharge, and  $m_t = 0.55$ ,  $f^{\text{Yield}} = 0.71$ ,  $f^{\text{Return}} = 0.46$  for the HiPIMS (low  $B$ ) discharge, respectively. Therefore, as one can see in figure 4, the *return effect* is a crucial phenomenon reducing  $M_r$  in HiPIMS (high  $B$ ) discharges. Note that the *yield effect* is very low in this case, mainly due to comparable  $U_{da}^{\text{HiPIMS}}$  and  $U_d^{\text{DCMS}}$  values (see figure 3). On the other hand, both *yield* and *return effects* need to be considered in the case of HiPIMS (low  $B$ ) discharges.

**3.2.3. Transport of the sputtered material.** In the previous two sections, we have identified and even quantified several phenomena affecting the sputtered material loss in the proximity of and/or at the target. In this section, we investigate transport of the sputtered material towards the substrate.

For this reason, Nb coating depositions were carried out onto silicon stripes fixed parallel and perpendicular with respect to the target surface (see figure 1), using the three previously discussed discharge conditions. As a result (shown in figure 5), one can obtain the normalized (with respect to

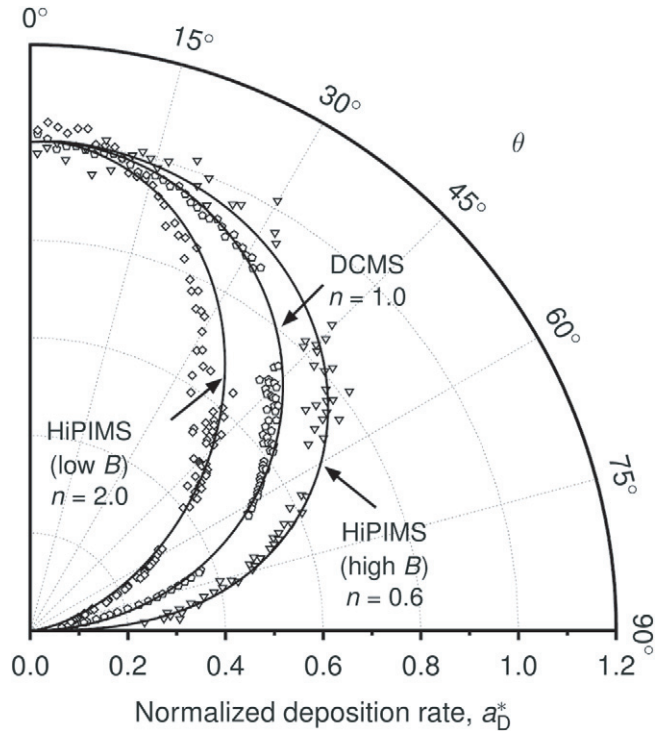


**Figure 5.** Measured data (open symbols) and the theoretical model [20] (solid lines) of the angular distribution of the normalized deposition rate,  $a_D^*$ , for the three investigated discharges operated at a constant average target power density in a period  $\bar{P}_d = 25 \text{ W cm}^{-2}$ . Zero degrees ( $\theta = 0^\circ$ ) stands for the sample position facing the centre of the target.

the centre of the substrate holder) deposition rate,  $a_D^*$ , as a function of  $\theta$ , which is the angle between the deposition direction (with respect to the target centre) and the magnetron's axis of symmetry. The experimental data were subsequently fitted using the model proposed by Fan [20], which is based on a formula describing the coating thickness,  $d_c$ , corresponding to a silicon stripe point,  $S_p$ , (see figure 1) as

$$d_c(S_p) = \int_0^{2\pi} \int_0^R E(r) \cos^n(\vartheta) \frac{r}{c^2} |\hat{c} \cdot \hat{n}| dr d\varphi. \quad (13)$$

Here,  $R$  is the target radius;  $E(r)$  is the function describing target erosion rate in a target point,  $T_p$ , at a radial distance from the target centre,  $r$ ; the expression,  $\cos^n(\vartheta)$ , represents the spatial distribution characteristic of sputtered atoms, where  $\vartheta$  stands for the angle between the sputtered particle direction and the surface normal, and  $n$  is a constant;  $c$  is the distance between points  $T_p$  and  $S_p$ ;  $\hat{c}$  is the unit vector in the direction from  $T_p$  to  $S_p$ ; finally,  $\hat{n}$  is the unit normal vector at point  $S_p$ . Integration over the whole target surface (represented by the distance  $r$  and by the angle in the target surface plane,  $\varphi$ ) guarantees that the contribution of every point  $T_p$  to  $d_c(S_p)$  is taken into account.

The resulting fit of the experimental data enables us to represent the angular distribution of the normalized deposition rate, using only one parameter:  $n$ . The higher the  $n$ , the more directional the deposition flux will be. In the three investigated cases we have (i)  $n = 1.0$  for DCMS discharge, (ii)  $n = 0.6$  for the HiPIMS (high  $B$ ) discharge and (iii)  $n = 2.0$  for

the HiPIMS (low  $B$ ) discharge. Indeed, in comparison with DCMS, the  $a_D^*$  profile of the HiPIMS (high  $B$ ) discharge suggests an enhanced flux of the sputtered material sideways (towards the chamber walls). In contrast, the HiPIMS (low  $B$ ) discharge is more focused towards the substrate facing the target (more directional regime).

The transport of the sputtered target matter is of fairly complex nature, particularly in HiPIMS, due to the high degree of ionization. In fact, both neutral atoms and ions exhibit various transport mechanisms [10, 12, 21–25]. In particular, the investigations by Lundin *et al* [10] and Poolcharuansin *et al* [24] showed that the propagation of ionized species can be largely affected by plasma instabilities, as in the case of anomalous ion transport across magnetic field lines. This behaviour could potentially explain our experimental observations at high  $B$ , since the elevated instantaneous target current densities may give rise to a substantial azimuthal ion transport towards the sides of the deposition chamber, and hence cause an increased deposition rate at the chamber walls perpendicular to the target. Other effects may be important under low  $B$  conditions, such as, the reported forward acceleration of the ionized sputtered species indicating the existence of a potential slope in between the dense plasma region and the substrates facing the target [25]. Indeed, the presence of such a potential profile within the HiPIMS discharge operated above a 75 mm diameter Nb target has recently been confirmed by Rauch *et al* [26]. In addition, the exponent  $n$  describing the spatial distribution characteristic of all sputtered atoms may be increased with a rise in the energy of impacting ions [19, 27].

Detailed understanding of all phenomena influencing the sputtered material transport in HiPIMS is beyond the scope of this paper. Nevertheless, the comparison of the angular distributions of the normalized (divided by  $a_D$  value for  $\theta = 0$ ) deposition rate, presented in figure 5, enables us to identify and quantify the *transport effect* (represented by the  $f^{\text{Transport}}$  coefficient) on the forward deposition rate. In fact,  $f^{\text{Transport}}$  is determined from the following condition:

$$\begin{aligned} f^{\text{Transport}} \int_0^{2\pi} \int_0^{\pi/2} a_D^*(\text{HiPIMS}) \sin(\theta) d\theta d\varphi \\ = \int_0^{2\pi} \int_0^{\pi/2} a_D^*(\text{DCMS}) \sin(\theta) d\theta d\varphi. \end{aligned} \quad (14)$$

Note that a more directional deposition flux implies a higher value of  $f^{\text{Transport}}$  and a lower value of the integral of  $a_D^*$  (see figure 5). We find that  $a_D$  in the centre of the substrate holder is reduced by 13% ( $f^{\text{Transport}} = 0.87$ ) in the case of the HiPIMS (high  $B$ ) discharge, while it is enhanced by 27% ( $f^{\text{Transport}} = 1.27$ ) in the case of the HiPIMS (low  $B$ ) discharge, if compared with DCMS.

**3.2.4. Coating growth at the substrate level.** In the following, we will conclude the findings of the previous sections (3.2.1–3.2.3) by a comprehensive summary, where all the aforementioned phenomena affecting  $a_D$  will be considered. First, it is to be stressed that no significant change in the coating density was observed (results not presented here). Also, no substrate etching or sticking coefficient reduction is

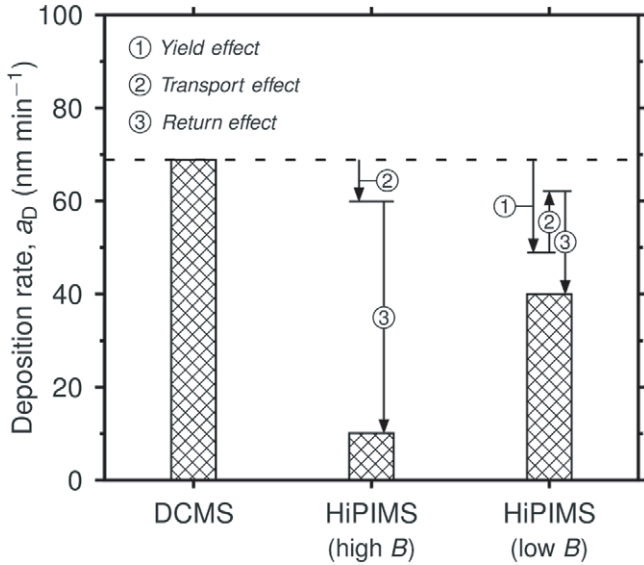


**Figure 6.** Deposition rate of Nb coatings  $a_D$  for the three selected discharges, operated at a constant average target power density in a period  $\overline{P_d} = 25 \text{ W cm}^{-2}$ . The respective contributions of *yield*, *transport* and *return effects* to  $a_D$  are indicated for both HiPIMS discharges.

expected under the present conditions (RF bias of  $-20 \text{ V}$ ). Therefore, *coating effects* ((v) in section 1) were supposed to be negligible, and were not taken into account.

Figure 6 presents the deposition rate of Nb coatings obtained by the three studied discharges and measured in the centre of the substrate holder. The principal contributions of *yield*, *return* and *transport effects* are also highlighted. In parallel to the discussion on the target mass loss analysis introduced in section 3.2.2, one can express the deposition rate in the case of HiPIMS discharges (considering there is no *return effect* in DCMS) as

$$a_D(\text{HiPIMS}) = a_D(\text{DCMS}) f^{\text{Yield}} f^{\text{Transport}} (1 - f^{\text{Return}}). \quad (15)$$

Here,  $a_D(\text{DCMS})$  is the deposition rate of the DCMS discharge operated at the same average target power density in a period  $\overline{P_d} = 25 \text{ W cm}^{-2}$  as HiPIMS discharges. Equation (15) allows us to determine, once again, the value of  $f^{\text{Return}}$  (using the corresponding  $m_t$  parameter calculated in section 3.2.2):  $f^{\text{Return}} = 0.83$  for the HiPIMS (high  $B$ ) discharge, and  $f^{\text{Return}} = 0.36$  for the HiPIMS (low  $B$ ) discharge. It is to be stressed that these values are (despite the complexity of the experiment) in good agreement with the values obtained from the target rate analysis based on the target mass measurement (discussed in section 3.2.2). The values of all the important variables and of the derived parameters used in this study are summarized in table 1.

As illustrated in figure 6, a significant amount of sputtered matter is lost due to the *return effect* under both conditions investigated. In fact, the *return effect* is the most important phenomenon lowering  $a_D$  in the HiPIMS (high  $B$ ) discharge. Instead, the use of lower  $B$  notably reduces this effect. However, the concurrent contributions of *return*, *yield* and *transport effects* result in a drop in  $a_D$  under low  $B$  conditions as well.

### 3.3. Ionized fraction of the deposition flux onto the substrate

A great advantage of the HiPIMS technique is the high ionized fraction of the deposition flux. It is somewhat natural to expect that the level of the sputtered material ionization is significantly altered by the differing discharge conditions corresponding to high or low values of  $B$  at constant  $P_{da}$ . In order to verify this expectation, we have characterized the plasma composition at the target and at the substrate levels using optical emission spectroscopy (OES).

Firstly, we will analyse the averaged OES data recorded for the three investigated discharges at a distance of  $d = 1 \text{ cm}$  (figure 7(a)) and of  $d = 9 \text{ cm}$  (figure 7(b)). In contrast to the DCMS spectrum, where lines due to excited neutral Nb and Ar are predominant, the two HiPIMS spectra (for both  $d$  values) show a significant presence of emission lines originating from the ionized Nb species. More interestingly, there is an important difference between the HiPIMS spectra detected at the two extreme magnetic field strengths. The HiPIMS (low  $B$ ) discharge is dominated by the emission from  $\text{Nb}^0$  and  $\text{Nb}^+$  lines, while significant  $\text{Ar}^+$  and strong  $\text{Ar}^0$  emissions are observed in the spectra of the HiPIMS (high  $B$ ) discharge at  $d = 9 \text{ cm}$ . It should be noted that similar notable  $\text{Ar}^+$  emission, accompanied by Nb lines depletion, was previously reported by the authors for HiPIMS discharges operated above an oxidized Nb target in  $\text{O}_2/\text{Ar}$  gas mixtures characterized by comparable power and current densities to the HiPIMS (high  $B$ ) discharge used here [14].

The latter observations may indicate a lower amount of sputtered Nb within the probed plasma volume, as well as more efficient Ar excitation, under the high  $B$  conditions. This may be interpreted as a consequence of the important *return effect* (83% of the sputtered material is returned back in this case, see section 3.2.2), if we assume that the average trajectory length of the returned target ions is much lower than target-to-probe distance (1 cm in this case). In such a case, the background gas (Ar) rarefaction effect [28] in front of the probe is suppressed, despite a very high instantaneous target power density. However, detailed investigations are necessary to clarify this interesting observation.

Figure 8 shows the emission intensity ratio

$$\kappa = \frac{I(\text{Nb}^+)}{I(\text{Nb}^0)}, \quad (16)$$

which is evaluated using two specific emission lines that have comparable energy levels of their upper excited states,  $E_k(\lambda_{\text{Nb}^0} = 467 \text{ nm})$  ranges from 2.9 to 4.2 eV and  $E_k(\lambda_{\text{Nb}^+} = 313 \text{ nm})$  equals 4.4 eV [29].  $\kappa$  thus represents an estimate of the degree of target material ionization, if we suppose that the selected  $\text{Nb}^0$  and  $\text{Nb}^+$  emitting species are only populated by electron impact excitation from the ground state, and only depleted by radiation.

As expected,  $\kappa$  corresponding to any of the HiPIMS spectra reaches much higher values ( $\kappa > 1$ ) than in the case of the DCMS discharge ( $\kappa \approx 0$ ) at both target–probe positions. Furthermore,  $\kappa$  at the target level is significantly higher in the case of HiPIMS (high  $B$ ) discharge ( $\kappa = 2.8$ ), when compared with the low  $B$  conditions ( $\kappa = 1.1$ ). This

**Table 1.** Summary of all the important experimental variables (*a*) and of the derived parameters (*b*) for the DCMS discharge and for the two selected HiPIMS discharges (i.e., high and low magnetic field strengths at the target surface), all operated at a constant average target power density in a period  $\bar{P}_d = 25 \text{ W cm}^{-2}$ . Note that  $f^{\text{Return}}$  and  $f^{\text{Return}^*}$  stand for the return probability derived in sections 3.2.2 and 3.2.4, respectively.

(a)	$ B_r $ (G)	$U_d$ (kV)	$U_{da}$ (kV)	$\bar{J}_d$ (mA cm $^{-2}$ )	$J_{da}$ (A cm $^{-2}$ )	$\bar{P}_d$ (W cm $^{-2}$ )	$P_{da}$ (kW cm $^{-2}$ )	$M_r$ (mg cm $^{-2}$ )	$a_D$ (nm min $^{-1}$ )
DCMS (low $B$ )	777	0.53	—	47	—	25	—	22.3	68.9
HiPIMS (high $B$ )	1031	—	0.48	52	5.20	25	2.5	3.7	10.1
HiPIMS (low $B$ )	777	—	1.42	17.6	1.76	25	2.5	8.5	40.0
(b)	$Y_{mg}$	$Y_{mm}$	$m_t$	$f^{\text{Yield}}$	$f^{\text{Transport}}$	$f^{\text{Return}}$	$f^{\text{Return}^*}$		
DCMS (low $B$ )	0.63	—	0	1	1	0	0		
HiPIMS (high $B$ )	0.59	0.54	0.47	0.99	0.87	0.83	0.83		
HiPIMS (low $B$ )	1.13	1.24	0.55	0.71	1.27	0.46	0.36		

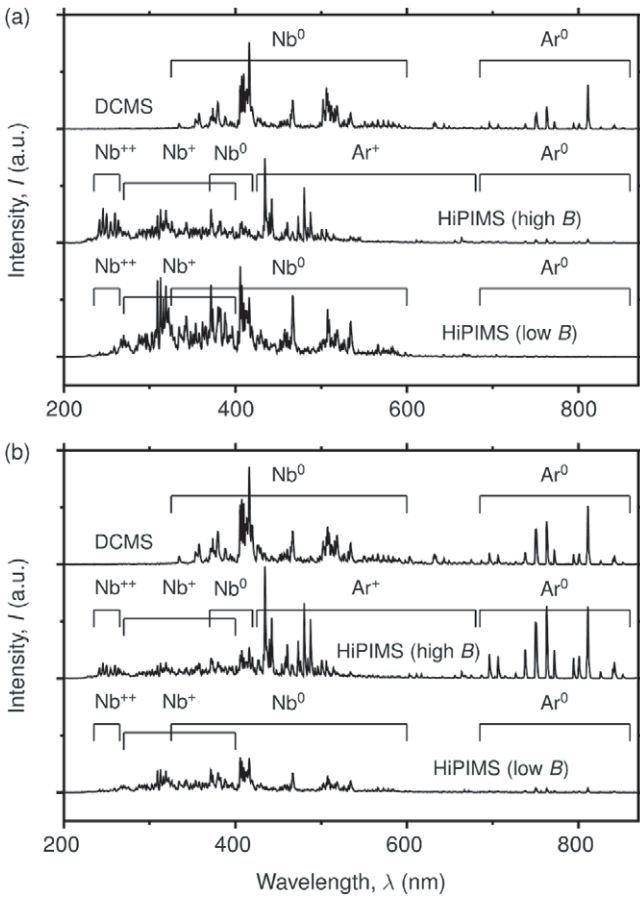


**Figure 7.** Optical emission spectra for the three selected discharges, operated at a constant average target power density in a period  $\bar{P}_d = 25 \text{ W cm}^{-2}$ . The optical emission probe was situated at  $d = 1 \text{ cm}$  (*a*) and at  $d = 9 \text{ cm}$  (*b*) from the target surface. The emission spectra at  $d = 1 \text{ cm}$  had an intensity about 14 times higher than their respective counterparts at  $d = 9 \text{ cm}$ .

observation is anticipated since it can be interpreted by the higher plasma density reached at high  $B$ . However,  $\kappa$  at the substrate level exhibits surprisingly similar value ( $\kappa \approx 1.0$ ) for both HiPIMS discharges under investigation. The particle flux towards the substrate,  $\Gamma_p$ , is proportional to the velocity of the particles and to the respective value of  $I$ . Assuming that the velocities of ion and neutral particles impacting on the substrate are not influenced by the change

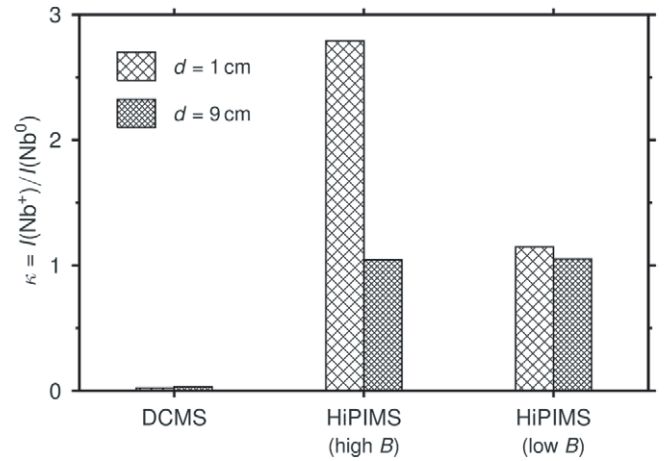


**Figure 8.** Ionized fraction of the sputtered material for the three investigated discharges, operated at a constant average target power density in a period  $\bar{P}_d = 25 \text{ W cm}^{-2}$ , estimated from OES analysis. The optical emission probe was situated at  $d = 1 \text{ cm}$  and  $d = 9 \text{ cm}$  from the target surface level.

in  $B$ , one can conclude that the degree of the deposition flux ionization  $\Gamma_p(\text{Nb}^+)/\Gamma_p(\text{Nb}^0)$ , and analogically also the ionized fraction of the deposition flux onto the substrate (discussed in the subsequent section), defined as

$$\Theta = \frac{\Gamma_p(\text{Nb}^+)}{\Gamma_p(\text{Nb}^+) + \Gamma_p(\text{Nb}^0)} \quad (17)$$

are comparable at both magnetic field configurations (high  $B$  and low  $B$ ). This is quite unexpected since one observes a fourfold increase in the deposition rate in the case of the HiPIMS (low  $B$ ) discharge! In the following section, we will elaborate on a possible explanation of this surprising result.

### 3.4. Theoretical analysis of the observed results

Vlček and Burcalová [15] derived detailed formulae for the power-normalized deposition rate  $a_D/P_{da}$  and the ionized fraction of the deposition flux onto the substrate  $\Theta$  in a steady-state high-power magnetron sputtering discharge. We will now apply it to our average characteristics of the HiPIMS discharges with long pulses.

Assuming, for simplicity, an identical loss probability of target material ions and neutrals to chamber walls during their transfer to the substrate and zero probability of additional ionization of sputtered atoms in the plasma bulk (i.e.,  $\xi_i/\xi_n = 1$  and  $\gamma = 0$  in the original work [15]), we obtain

$$\frac{a_D}{P_{da}} \propto (1 - \beta\sigma) \frac{U_{da}^{-0.5}}{1 + \gamma_{se}} \quad (18)$$

and

$$\Theta = \frac{\beta(1 - \sigma)}{1 - \beta\sigma}. \quad (19)$$

The assumption  $\xi_i/\xi_n = 1$  is not necessarily true as it was discussed in section 3.2.3; however, it will not compromise the conclusions in this section while making the argumentation clearer.

A balance equation for secondary electrons (see equation (8) in the original work [15]) enables one to determine a relation between the return probability and the magnetron voltage as

$$\sigma \propto \frac{1}{U_{da}}. \quad (20)$$

One can also assume that secondary electrons govern the ionization process in front of the target [15, 30, 31], thus we can write

$$\beta \propto N_{iz}n_{se}. \quad (21)$$

Here, the number of collisional ionizations of each secondary electron with the sputtered atoms,  $N_{iz}$ , can be estimated as  $N_{iz} = (eU_{da})/E$ , where  $E$  is the energy lost per electron–ion pair produced. In addition, the density of secondary electrons,  $n_{se}$ , scales as  $n_{se} \propto \gamma_{se}\Gamma_{ita}$ , where  $\Gamma_{ita}$  is the average pulse ion flux onto the target. Since the value of  $\Gamma_{ita}$  is directly proportional to  $J_{da}$ , we find the scaling  $\beta \propto U_{da}J_{da} = P_{da}$ .

Taking into account that the  $P_{da}$  value was fixed in the present experiments (hence  $\beta$  is constant), and that  $\sigma \propto 1/U_{da}$  and  $\gamma_{se} \ll 1$ , it is seen from equation (18) that a significant rise in  $U_{da}$  (at lower  $B$ ) leads to an increase in  $a_D/P_{da}$ , due to a lower value of  $\sigma$ . In addition, equation (19) indicates that  $\Theta$  remains almost unchanged due to the high value of  $\beta$ , corresponding to the elevated  $P_{da} \simeq 2.5 \text{ kW cm}^{-2}$ . The high value of  $\beta$  is also supported by the experimental data. If we consider that  $\beta\sigma = 0.83$  for the HiPIMS (high  $B$ ) discharge (discussed in section 3.2.2), and that  $\beta \propto P_{da}$ , we can conclude that  $\beta \geq 0.83$  for both HiPIMS discharges.

The theoretical discussion above therefore shows, among other findings, that  $\sigma$  is the key parameter determining the ratio of the backward (towards the target) and of the forward (towards the substrate) target material ion fluxes. A decrease in the magnetic field strength leads to a decrease in the backward flux of ions due to a lower  $\sigma$  corresponding to a higher  $U_{da}$  (equation (20)), which is necessary to keep  $P_{da}$  constant. Subsequently, a higher portion of the ions generated close to the target becomes available for deposition onto the substrate.

## 4. Summary and conclusions

In this paper, we investigated the concept of the deposition rate  $a_D$  enhancement of Nb coatings prepared by HiPIMS through the control of the magnetron's magnetic field strength at the target surface,  $B$ . We found that lowering  $B$  results in a significant increase in  $a_D$  by a factor of up to  $\sim 4.5$  (from 10.6 to 45.2 nm min<sup>-1</sup>), when compared with the high  $B$  configurations. Nevertheless, the ionized fraction of the deposition flux onto the substrate was found to be comparable, despite a large difference in discharge characteristics (magnetron voltage and discharge current). Moreover, we demonstrated that the observed behaviour may be a general feature of HiPIMS discharges.

The maximum  $a_D$  value was found to be about 33% lower in comparison with the (non-pulsed) dc magnetron sputtering operated at an identical average power. This observation is due to the physical limitations described here. Specifically we have demonstrated that the deposition rate reduction is governed by different phenomena, depending on  $B$ : (i) the attraction of the target ions back to the target is the dominant effect at high values of  $B$ , while (ii) the sub-linear dependence of the sputtering yield on the ion energy, the target ions' back-attraction towards the target, and the variations in the sputtered material transport, all need to be considered under low  $B$  conditions.

Based on the present understanding, we propose that there are still other pathways for further  $a_D$  enhancement that have not been explored in this work. For example, one can profit from the fact that it takes some time for the *return effect* to develop, such as previously suggested by Konstantinidis *et al* [32].

## Acknowledgments

The authors wish to thank Professor Jaroslav Vlček, Dr Šimon Kos and Dr Tomáš Kozák for valuable discussions, and Mr Francis Turcot and Mr Sébastien Chenard for their expert technical assistance. The financial support of NSERC of Canada within the CRDPJ 380174-08 project is gratefully acknowledged.

## References

- [1] Sarakinos K, Alami J and Konstantinidis S 2010 High power pulsed magnetron sputtering: a review on scientific and engineering state of the art *Surf. Coat. Technol.* **204** 1661
- [2] Gudmundsson J T, Brenning N, Lundin D and Helmersson U 2012 High power impulse magnetron sputtering discharge *J. Vac. Sci. Technol. A* **30** 030801
- [3] Lundin D and Sarakinos K 2012 An introduction to thin film processing using high-power impulse magnetron sputtering *J. Mater. Res.* **27** 780
- [4] Helmersson U, Lattemann M, Alami J, Bohlmark J, Ehasarian A P and Gudmundsson J T 2005 High power impulse magnetron sputtering discharges and thin film growth: a brief review *Society of Vacuum Coaters 48th Annual Technical Conf. Proc.* (Denver, CO, 23–28 April 2005) p 458

- [5] Samuelsson M, Lundin D, Jensen J, Raadu M A, Gudmundsson J T and Helmersson U 2010 On the film density using high power impulse magnetron sputtering *Surf. Coat. Technol.* **205** 591
- [6] Vlček J, Zuštin B, Rezek J, Burcalová K and Tesař J 2009 Pulsed magnetron sputtering of metallic films using a hot target *Society of Vacuum Coaters 52th Annual Technical Conf. Proc.* (Santa Clara, CA, 9–14 May 2009) p 219
- [7] Emmerlich J, Mráz S, Snyders R, Jiang K and Schneider J M 2008 The physical reason for the apparently low deposition rate during high-power pulsed magnetron sputtering *Vacuum* **82** 867
- [8] Christie D J 2005 Target material pathways model for high power pulsed magnetron sputtering *J. Vac. Sci. Technol. A* **23** 330
- [9] Anders A 2010 Deposition rates of high power impulse magnetron sputtering: physics and economics *J. Vac. Sci. Technol. A* **28** 783
- [10] Lundin D, Larsson P, Wallin E, Lattemann M, Brenning N and Helmersson U 2008 Cross-field ion transport during high power impulse magnetron sputtering *Plasma Sources Sci. Technol.* **17** 035021
- [11] Ehiasarian A P and Vetushka A 2009 Magnetron configuration to enhance deposition rate in high power impulse magnetron sputtering *Society of Vacuum Coaters 52th Annual Technical Conf. Proc.* (Santa Clara, CA, 9–14 May 2009) p 265
- [12] Mishra A, Kelly P J and Bradley J W 2010 The evolution of the plasma potential in a HiPIMS discharge and its relationship to deposition rate *Plasma Sources Sci. Technol.* **19** 045014
- [13] Glowacki B A, Yan X-Y, Fray D, Chen G, Majoros M and Shi Y 2002 Niobium based intermetallics as a source of high-current/high magnetic field superconductors *Physica C* **372–376** 1315
- [14] Hála M, Čapek J, Zabeida O, Klemberg-Sapieha J E and Martinu L 2012 Hysteresis-free deposition of niobium oxide films by HiPIMS using different pulse management strategies *J. Phys. D: Appl. Phys.* **45** 055204
- [15] Vlček J and Burcalová K 2010 A phenomenological equilibrium model applicable to high-power pulsed magnetron sputtering *Plasma Sources Sci. Technol.* **19** 065010
- [16] Čapek J, Hála M, Zabeida O, Klemberg-Sapieha J E and Martinu L 2012 Steady state discharge optimization in high-power impulse magnetron sputtering through the control of the magnetic field *J. Appl. Phys.* **111** 023301
- [17] Hála M, Viau N, Zabeida O, Klemberg-Sapieha J E and Martinu L 2010 Dynamics of reactive high-power impulse magnetron sputtering discharge studied by time- and space-resolved optical emission spectroscopy and fast imaging *J. Appl. Phys.* **107** 043305
- [18] Mutzke A, Schneider R, Eckstein W and Dohmen R 2011 SDTrimSP Version 5000 *Report IPP 12/8*, Garching
- [19] Westwood W D 2003 *Sputter Deposition* (New York: AVS)
- [20] Fan Q, Chen X and Zhang Y 1995 Computer simulation of film thickness distribution in symmetrical magnetron sputtering *Vacuum* **46** 229
- [21] Bohlmark J, Östbye M, Lattemann M, Ljungcrantz H, Rosell T and Helmersson U 2006 Guiding the deposition flux in an ionized magnetron discharge *Thin Solid Films* **515** 1928
- [22] Ehiasarian A P, Andersson J and Anders A 2010 Distance-dependent plasma composition and ion energy in high power impulse magnetron sputtering *J. Phys. D: Appl. Phys.* **43** 275204
- [23] Brenning N, Huo C, Lundin D, Raadu M A, Vitelarú C, Stancu G D, Minea T and Helmersson U 2012 Understanding deposition rate loss in high power impulse magnetron sputtering: I. Ionization-driven electric fields *Plasma Sources Sci. Technol.* **21** 025005
- [24] Poolcharuansin P, Liebig B and Bradley J W 2012 More evidence for azimuthal ion spin in HiPIMS discharges *Plasma Sources Sci. Technol.* **21** 015001
- [25] Horwat D and Anders A 2010 Ion acceleration and cooling in gasless self-sputtering *Appl. Phys. Lett.* **97** 221501
- [26] Rauch A, Mendelsberg R J, Sanders J M and Anders A 2012 Plasma potential mapping of high power impulse magnetron sputtering discharges *J. Appl. Phys.* **111** 083302
- [27] Wehner G K and Rosenberg D 1960 Angular distribution of sputtered material *J. Appl. Phys.* **31** 177
- [28] Rossnagel S M 1988 Gas density reduction effects in magnetrons *J. Vac. Sci. Technol. A* **6** 19
- [29] Kurucz R L and Bell B 1995 Atomic line data, Kurucz CD-ROM, No 23, Cambridge, MA
- [30] Lieberman M A and Lichtenberg A J 2005 *Principles of Plasma Discharges and Materials Processing* (New York: Wiley-Interscience)
- [31] Kozák T and Pajdarová A D 2011 A non-stationary model for high power impulse magnetron sputtering discharges *J. Appl. Phys.* **110** 103303
- [32] Konstantinidis S, Dauchot J P, Ganciu M, Ricard A and Hecq M 2006 Influence of pulse duration on the plasma characteristics in high-power pulsed magnetron discharges *J. Appl. Phys.* **99** 013307